The Iron K Line Analysis of Clusters of Galaxies Observed with ASCA

F. Akimoto[1,2], A. Furuzawa[1], Y. Tawara[1], K. Yamashita[1]
[1] *Department of Physics, Nagoya University*
[2] *Research Center for Advanced Energy Conversion, Nagoya University*

Abstract

ASCA observations of some nearby cool clusters of galaxies make it clear that they have larger iron Kβ line intensities than ones expected from plasma temperatures and iron Kα line intensities. For each hot cluster of galaxies, because line intensity is small, this phenomenon is not clear. Therefore, 150 clusters of galaxies are classified within 5 groups according to plasma temperature and all spectra of each group are summed after correction of redshift. These spectra show iron line intensities are affected by the effect of resonance scattering (optical depth is about 2). Moreover, summed SIS spectra revealed the He-like iron Kβ line and H-like iron Kβ line. The interpretation of these line intensities needs the effects of the resonance scattering. This means the iron abundances driven from He-like iron Kα are underestimated at the center of clusters of galaxies, if this effect is not corrected. The correction of this effect is inclined to strengthen the concentration of abundance at the center of galaxy clusters and to make the variety of abundance of each galaxy cluster large.

1 Statistical Analysis of Galaxy Clusters

We analysed 150 clusters of galaxies observed with $ASCA$ (including group of galaxies 20%, binary galaxies a few %, galaxy 10%) using common manner to minimize systematic deviation due to instrumental characteristics.

1.1 Targets

No selection of targets has done because our aim is to analysis all clusters of galaxies observed with $ASCA$ at common methods. Therefore, as shown in luminosity Lx of 2 – 10 keV energy band vs. redshift z relation (figure 1.1), the list of targets is including clusters of galaxies with various size, various redshift and various Lx ranging over 5 order. Moreover, some of them have bright symmetric distributions of surface brightness, and some have irregular brightness distributions without clear core regions. At the latter case, it is difficult to analysis with common methods. For example,

because there are some X-ray peaks associated with member galaxies in addition to X-ray emission of galaxy cluster component, it is difficult to determine the center of X-ray emission. Then, we analysed at especially methods such as the size of smoothing is large. The detection limit for $ASCA$ is also shown in this figure.

Figure 1.1 : Correlation of Lx and z

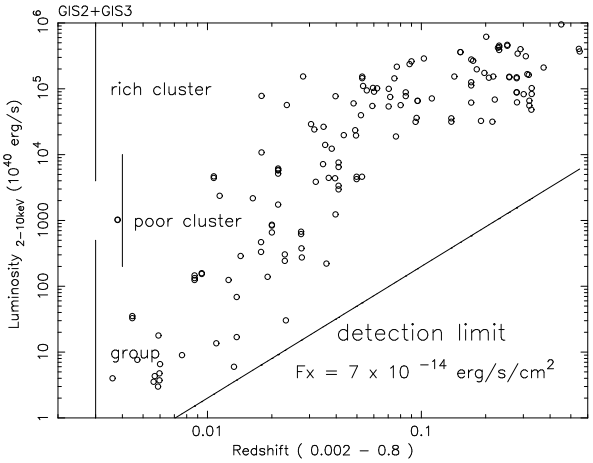

Range of obtained parameters

Lx : 10^{40-46} erg s^{-1}
kT : 0.7 – 12 keV
abundance : 0.07 – 0.6 solar
$R_c \leq$ 300 kpc
β : 0.3 – 0.9
M_{tot} $(r < 3R_c)$: 10^{12-16} $M_\odot$
M_{gas} $(r < 3R_c)$:10^{10-15} $M_\odot$
f_{gas} $(r < 3R_c)$: 0.01 – 0.3

1.2 Analysis

1.2.1 Images

Observed $ASCA$ X-ray images are distorted by Point Spread Function (PSF) of X-ray telescope. Then, low band (0.7 – 1.5 keV) GIS images were deconvoluted by PSF using IDL soft (Lucy Algorithm). Here, 3C273 images observed with $ASCA$ were used for PSF. The radial profiles of surface brightness whose center positions are the X-ray peaks were made from deconvoluted images, assuming the cluster of galaxies is symmetric. By using the β model and constant background for the fitting of the brightness profiles, core radius R_c and β are estimated.

1.2.2 Spectra

X-ray spectrum is accumulated within a circle whose center position coincides with the X-ray peak. The radius of the circle is defined to be the radius R_{90}, involving 90 % flux of clusters of galaxies. If the radius is larger than the FOV of detector, the radius which involves 90 % flux of the whole

of detected flux is used. The spectra of center region and the outer ring region are also accumulated. These regions are defined to be the central circle of the radius of 0.5 R_{90} and the outer ring region whose range of radius is from 0.5 R_{90} to R_{90}, respectively.
The spectra of energy band, 0.5 – 10 keV (SIS) and 0.7 – 10 keV (GIS) within these three regions are fitted with a model which consists of Raymond-Smith model and absorption model. Temperature kT, iron abundance, 2 – 10 keV luminosity Lx are obtained.

From image and spectral parameters, assuming the hydrostatic equilibrium, we estimated radial distribution of gas density and so on. The ranges of obtained parameters are shown in the right side of the figure 1.1. These values are used for calculations of optical depth in section 4.

2 Line Analysis of Each Galaxy Cluster

The 3 – 10 keV spectra of all 150 clusters are fitted with a model which consists of a bremsstrahlung and some Gaussian lines. Almost of obtained iron K_α and K_β line energies are 6.55 – 6.95 keV and 7.6 – 8.3 keV, and line center energies of He-like iron K_α and H-like iron K_α obtained from SIS data are 6.5 – 6.8 keV and 6.7 – 7.04 keV, respectively.

Figure 2.1 : Line intensity ratio of He-like iron K_α to H-like iron K_α (SIS)

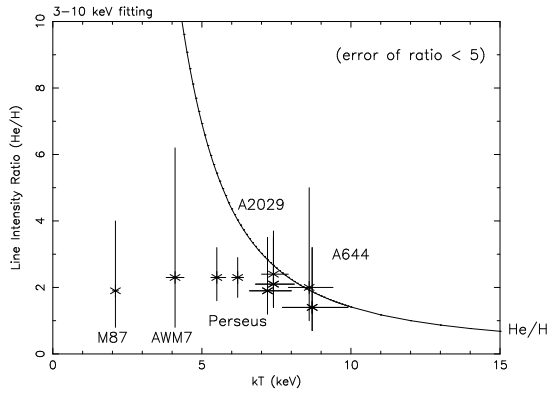

Concerning nearby galaxy clusters, such as M87, AWM7 and Perseus cluster, the iron K_α line intensity ratios of He-like iron K_α to H-like iron K_α ($= I_{\text{He-like Fe K}\alpha} / I_{\text{H-like Fe K}\alpha} \equiv R_2$) are not consistent with optically thin model as shown in figure 2.1. The optically thin model (Masai model) which is calculated from 19 He-like iron K_α lines and 4 H-like iron K_α lines is shown by a line. As the other clusters of galaxies have large errors of

ratios, the ratios are consistent with optically thin model. Nonetheless, $\sim$ 80 % of the clusters is inclined to have smaller ratios than the model. Moreover $\sim$ 80 % of clusters is inclined to have smaller intensity ratios of K_α line to K_β line ($= I_{K\alpha}$ / $I_{K\beta} \equiv R_1$) than the model value calculated from 23 K_α lines and 18 lines[1] for K_β line of Masai model.

3 Summation of Spectra and Line Analysis

3.1 Summation of Spectra

In order to study the typical properties of clusters of galaxies with similar X-ray properties, the obtained images (distributions of surface brightness) and spectra are summed. These results enable us to analysis images and spectra in details.

First, we divided all targets into 5 groups according to cluster temperature, 0 – 1, 1 – 3, 3 – 6, 6 – 9, 9 – 12 keV. Here, we excluded the targets of poor photon statistics, whose criterion is that the photons of He-like iron K_α line is less than 0.5 (cts cm^{-2}). The number of selected targets for each group are shown in the table 3.1.

Table 3.1 : Temperature range and number of selected targets (GIS)

temperature range (keV)	number of targets		
	all region	center region	ring region
1 - 3	8	8	8
3 - 6	33	32	24
6 - 9	28	22	13
9 - 12	14	16	17

Next, all spectra are corrected for $ASCA$ efficiency using unfolded spectrum of XSPEC package. At that time, a model without lines is assumed. Moreover, the redshift correction is also done. Then, we summed up these corrected spectra of all targets for each temperature group. Two of resultant spectra are shown in figure 3.1 by way of examples. Spectra of best photon statistics not only enabled to assess the effect of resonance scattering but also revealed He-like iron Kβ line and H-like iron Kβ line are detected respectively.

[1] 18 lines are including nickel lines, assuming that nickel abundance and iron abundance are 1 cosmic value.

Last, these spectra are fitted with continuum and Gaussian components, as shown in this figure. The model for GIS consists of continuum and two Gaussian lines, and one or two Gaussian lines are added for fitting of SIS spectra. The resultant values of line center energies and intensities are also shown in the figure 3.1.

Figure 3.1 : The summed 3 – 10 keV spectra for all region ($R < R_{90}$) of clusters of $kT > 6$ keV. The left panel is GIS spectrum and the right one is SIS spectrum. The X axis is Energy (keV) and Y axis is keV/cm^2 keV.

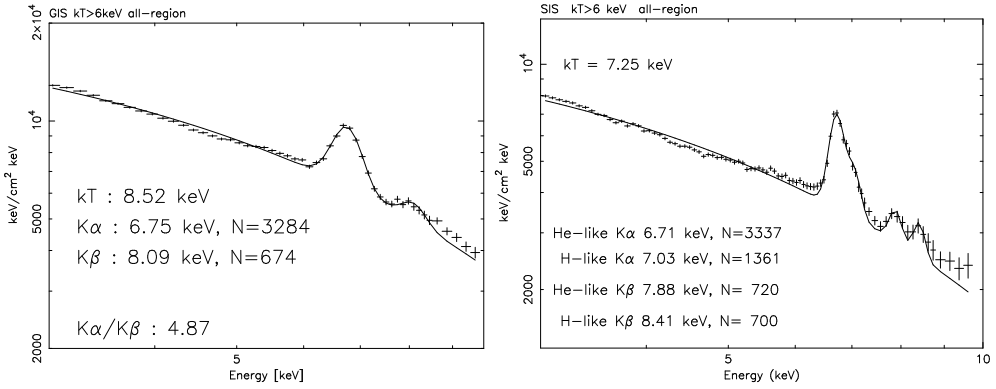

3.2 Line Energy

The deviations of observed line center energy from the optically thin model are shown in figure 3.2.

Figure 3.2 : Deviation of observed line center energy of each group from the Masai model. The left panel is for Kα and Kβ lines of GIS and the right one is for He-like iron Kα and H-like iron Kα line of SIS.

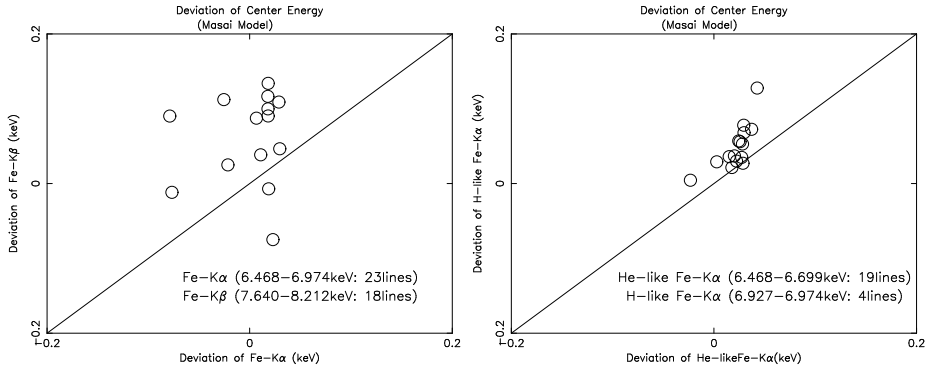

The differences of observed GIS data and the expected model are smaller than 100 eV at iron Kα line and 300 eV at iron Kβ line. The differences of SIS data are small (< 100 eV) at both of He-like iron Kα and H-like iron Kα line.
Moreover, the deviation of two lines for each detector is not similar. Therefore systematic error of spectral energy is negligible.
The deviations of Kβ line are large because the center energy probably increases due to existence of ~ 8.5 keV line.

3.3 Line Ratio

We estimated five line intensity ratios as follows,

$R_1 \equiv$ Kα-Blend / Kβ-Blend
$R_2 \equiv$ He-like iron Kα line / H-like iron Kα line
$R_3 \equiv$ He-like iron Kβ line / H-like iron Kβ line
$R_4 \equiv$ He-like iron Kα line / He-like iron Kβ line
$R_5 \equiv$ H-like iron Kα line / H-like iron Kβ line

Here, Kα-Blend consists of He-like iron Kα line and H-like iron Kα line, and Kβ-Blend consists of He-like iron Kβ line and H-like iron Kβ line.

These line intensity ratio is determined by only temperature. However, due to the limit of energy resolution of $ASCA$, He-like iron Kβ line includes nickel lines. Therefore, R_1, R_3 and R_4 are dependent on uncertainty of nickel abundance.
Furthermore, because observed H-like iron Kβ line may have iron Kγ, δ, ϵ lines (1s2S$-$4p2P: 8.7 keV, 1s2S$-$5p2P: 8.9 keV, 1s2S$-$6p2P: 8.9 keV), we must consider these high-energy lines into discussion of R_4 and R_5.
The ratio R_2 is determined by only temperature.

The line intensity ratios obtained from SIS data are shown as data points in figures 3.3 and 3.4. The temperature was estimated from continuum on the assumption of a single temperature.
The model ratios calculated from Masai94a model, which is for the optically thin plasma in the collisional equilibrium, are added with lines in these figures. In the figures of R_1 ratio, the model ratios which the effect of nickel lines are considered into are also shown. The cases of nickel abundance is 0, 1, 2, 3, 4 and 5 times larger than iron abundance are shown. In the

figure of R_3 and R_5, the model ratios that Kγ, δ, ϵ lines are included are also shown. Contributions of nickel in R_3 and R_4 are not shown in figures.

Figure 3.3 : Line ratios of center region (SIS) and optically thin models. The top left panel is R_1 and the top right one is R_2, the second one is R_3, the bottom left panel is R_4 and the bottom right panel is R_5.

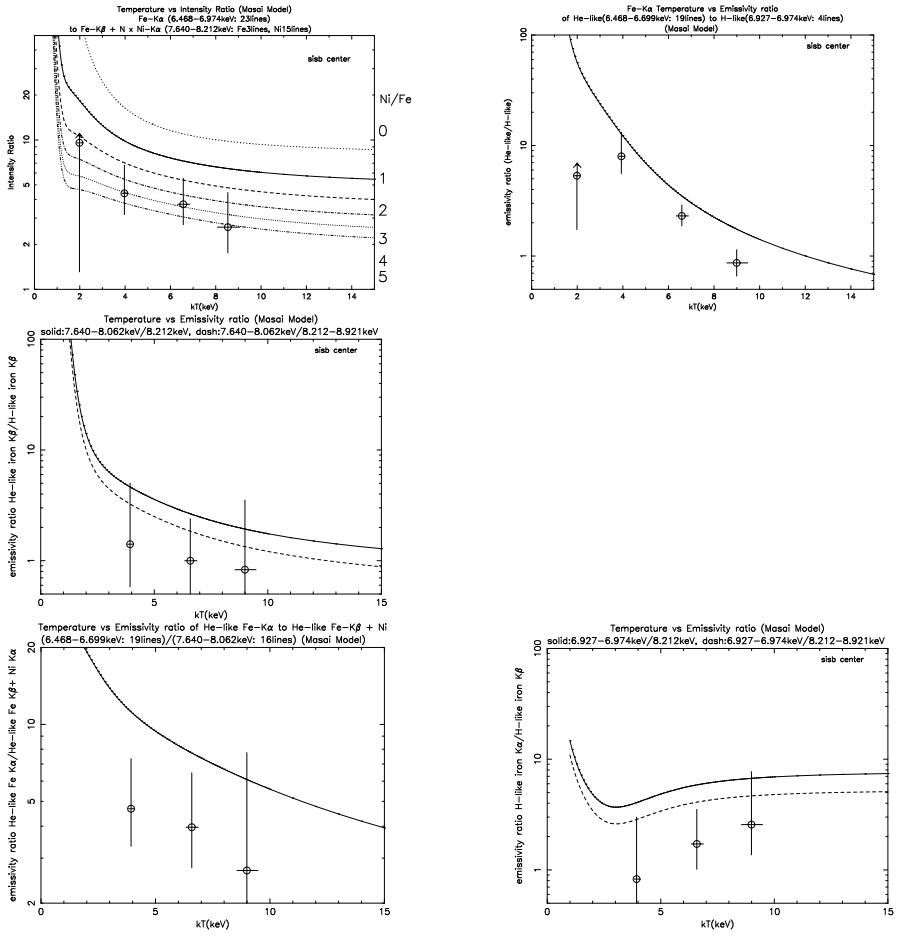

According to these figures, all observed line intensity ratios of center region are not consistent with continuum temperature. Then, we will discuss contribution of nickel line and iron Kγ and so on and effects of the resonance scattering as these origin in section 3.4. Moreover almost of the intensity ratios of center region are smaller than those of ring and all region.

With regard to the effect of resonance scattering, the case of $\tau = 0$, 1, 2, 3 and 5 and the integrated radius = 1/2 R_c are shown in figure 3.4. The resonance scattering are stated in section 4. As the R_3 is not affected by the resonance scattering, the figure of R_3 is not shown.

Figure 3.4 : Line ratios of center region (SIS) and effects of resonance scattering. The top left panel is R_1 and the top right one is R_2, the bottom left panel is R_4 and the bottom right panel is R_5.

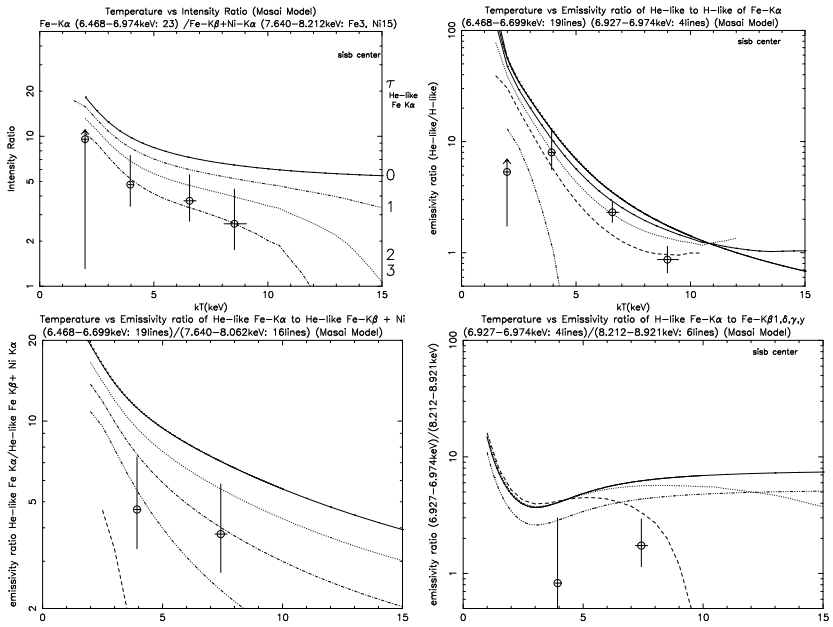

3.4 Summary of Results

3.4.1 R_1 ratio

The observed R_1 ratios of the central region are smaller than the model of optically thin plasma, but those of the outer region are consistent with the model. If the small ratios of central region must be explained by only the contribution of nickel, the nickel abundance needs to be $3^{1.0}_{-1.5}$ times larger than iron abundance. If the contribution of effects of the resonance scattering is considered, the τ of He-like iron K_α line is expected to be 2.5^{+1}_{-1} for central region. For the cool clusters ($kT < 3$ keV), the central value is very small though the error is large. The value implies that nickel abundance is ~ 5 times larger than iron abundance or τ of He-like iron K_α line is ~ 5.

3.4.2 R_2 ratio

The R_2 ratios are smaller than the model, except for the ratios of ring regions of the hot clusters ($kT > 9$ keV), whose ratio is larger than

model. This ratio is independent of nickel abundance. Therefore, this ratio demands τ of the resonance scattering is $2 \sim 3$.

3.4.3 R_3 ratio

The observed R_3 are consistent with the model, except for the ratios of all region of the cluster whose kT is less than 9 keV, although they have large errors.

3.4.4 R_4 ratio

The all of observed R_4 are smaller than the model. The ratios of ring region are inclined to be larger than that of center region.

3.4.5 R_5 ratio

The all of center values of observed R_5 are smaller than the model of optically thin plasma. The observed ratios of $6 - 9$ keV cluster are especially smaller than the model and the ratios of outer region are consistent with the model. Therefore the effect of resonance scattering seems to have to be considered.

4 The Effects of Resonance Scattering of Galaxy Clusters

Some of the stronger resonance lines of highly ionized heavy elements have relatively large absorption oscillator strength (e.q. $f_{12} > 0.1$) and are scattered by the ions[2]. Therefore, the optical depth of the resonance lines τ is hundreds or thousands of times larger than that of Thomson scattering $\tau_{\rm Th}$.
At the cluster center, since the gas density is high, resonance lines are scattered and observed to be suppressed [1]. The suppressed component is observed to be a significant enhancement in outer part of cluster. Therefore, the radial profile of surface brightness is distorted as shown in the left panel of figure 4.1. Eventually the total intensity over the whole cluster is not changed.

[2] An X-ray photon absorbed by a bound-bound transition of a certain ion is reemitted by a spontaneous radiative transition of the same ion and not destroyed by collisions with an electron or another ion because the ratio of the frequencies of the two processes is extremely high.

Figure 4.1 : Distortion of surface brightness and line profile

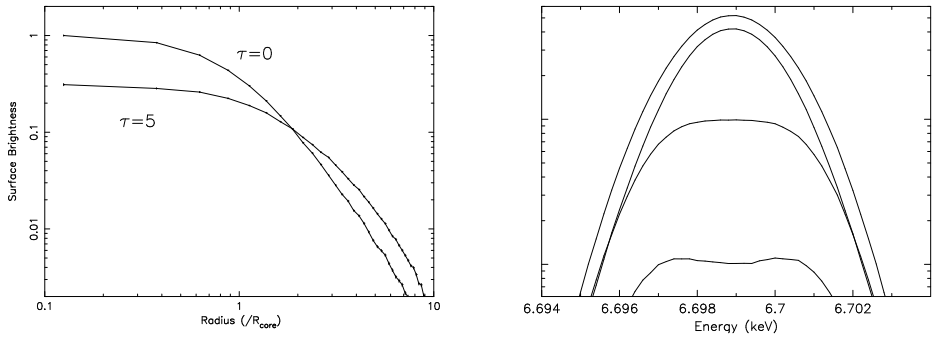

To understand the the resonance scattering at first sight, we demonstrate the results of Monte Carlo simulation in figure 4.1. In left panel, the resultant surface brightness profile of simulation at τ of 5 is shown with the profile of optically thin case. At the cluster center, large amount of photons of line emission are scattered and scattered photons are observed at outer region($R > 2\ R_c$). In right panel, the line profile of He-like iron Kα line at 2 keV galaxy cluster, whose R_c is 60 kpc and β is 0.86 is shown. Four lines show the difference of the integrated radius (all region, outer region; $R > R_c$, center region; $R < R_c$, smaller central region; $R < 0.1\ R_c$). A line emitted from cluster center ($< 0.1\ R_c$) has scattered most effectively and has saddle-shaped profile. On the contrary, that of outer region has sharper peak than that of whole region. Though this effect is not detected with $ASCA$ due to the energy resolution, the other effects are expected.

The amounts of scattered photons depend on the optical depth τ. τ at the midpoint of He-like iron Kα line at the cluster center is given by equation (1) using cross section $\sigma(T_e)$,

$$\tau_{He-likeFeK\alpha} = \int \sigma(T_e) n_{Fe} i_{XXV} dr \tag{1}$$

where n_{FeXXV}, n_{Fe}, n_H and n_e is the density of He-like iron, iron, hydrogen and electron, respectively, and then $i(T_e)$ denotes the ion fraction of the ionization state, XXV at temperature T_e.

$\sigma(T_e)$ at the energy center of a Doppler profile line due to the resonance scattering is expressed as,

$$\sigma(T_e) \sim 4.24 \times 10^{-17} f_{12} \frac{1}{E_0} \left(\frac{A}{kT_e}\right)^{\frac{1}{2}} \ (cm^2) \tag{2}$$

where, E_0 is the line center energy in keV and A is the atomic weight of the atom of radiating the line, kT_e is the plasma temperature of cluster of galaxies in keV.

Table 4.1 : optical depth of each cluster

target	τ	target	τ	target	τ
Cen	2.89	HYD-A	1.42	PKS0745−191	1.17
PER	1.99	A2390	1.35	A2199	1.17
M87	1.77	A478	1.27	A1795	1.16
A1704	1.72	A2204	1.25	AWM7	1.14
E1455	1.69	A1045	1.25	A262	1.12
A3112	1.67	A1204	1.21	A85	1.08
A496	1.57	A483	1.20	MKW3S	0.99
A1722	1.44	A115	1.19	A2029	0.99

We calculated τ at the midpoint of He-like iron Kα line on the center region of 150 clusters of galaxies using the results of our analysis (kT, abundance, central gas density) and Masai model. The results are summarized in table 4.1. It was made clear that optical depth of 22 clusters are larger than unity.

5 Discussion

The large intensity of iron Kβ line in comparison with He-like iron Kα is controversial topic.

Okumura *et al.* [2] investigated the intensity ratio of iron K_α to K_β of 3 clusters of galaxies with $TENMA$(non imaging) and showed observed ratios are lower than model in Coma and Ophiucus except for Perseus, but they concluded the effect of resonance scattering is no more effective. Molendi *et al.* [3] argued that the ratio is significantly smaller than model and increases with increasing cluster radius according to *Beppo-SAX*(MECS) of Perseus cluster because of resonant scattering. But Buote *et al.* [4] claimed that model is consistent with observed ratio, moreover if the gas is multiphase, Molendi *et al.*'s procedure is inappropriate because using a local continuum generally gives a larger temperature near the Fe XXV line than derived from a broad continuum. They also quoted $ASCA$ News ([5] is written, but [6] is correct) and claimed that structures of high energy band is due to $ASCA$ XRT instruments. However, the structures

in the quoted data is not real but is due to poor photon statistics. *ASCA* XRT can not make this high energy structures.

Dupke *et al.* [7] reported Ni $\sim$ 5 Fe on the basis of their results of *ASCA* data analysis of clusters which have concentrations of iron. They argued that the Ni is consistent with Convective Deflagration model = W7 SN Type Ia model [8] [9] and it suggests at the center of galaxy cluster, eject from SN Ia is large.
However, if nickel abundance is large ($\sim$ 5 Fe), R_3 is larger than optically thin model. Our analysis of line profile of iron Kβ suggests nickel abundance is lower than 1.8 times larger than iron abundance (solar). Moreover, nickel over abundance can not explain the small R_2 ratio.

6 Conclusion

We estimated 5 intensity ratios of iron K line of 150 galaxy clusters and made it clear that some cool clusters of galaxies have small R_1 and R_2, R_1 and R_2 is inclined to be smaller than models at the cluster center of $\sim$ 80% galaxy clusters thought errors are large, almost of 5 ratios obtained from summed spectra of center region are smaller than optically thin model and observed one of ring region.

From contribution of nickel to R_1, R_3 and R_4, abundance of nickel is lower than 1.8 times larger than iron abundance (solar).

R_3 and R_5 are consistent with contribution of iron Kγ lines and so on, and R_1, R_2 and R_4 is explained by the effect of the resonance scattering ($\tau \sim 2$).

Therefore, when we estimate abundances using He-like iron Kα line, we must consider the resonance scattering. On the other hand, obtained optical depth is used for

7 Feasibility

◯ *XMM*
XMM has large effective area, and enables us to determine line intensities, exactly. This means the line analysis makes good progress.

◯ *Chandra*
Since *Chandra* has high spatial resolution, spectra of central regions of galaxy clusters can be obtained. The line intensities of the spectra are most affected with the resonance scattering. If the correction of the scattering is not done, the abundances of center region are underestimated.

○ $ASTRO-E2$
This will have high energy resolution. The expected spectra are shown in figure 7.1. $ASTRO-E2$ will enable to determine nickel abundance exactly. Therefore, we can also estimate intensity of iron Kβ exactly.

Figure 7.1 : Effect of nickel

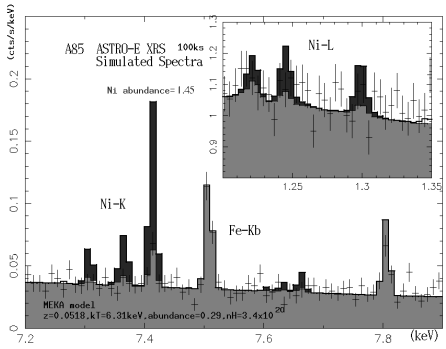

If τ of the resonance scattering is estimated from observed spectrum, we can calculated the Hubble constant. Percentage of error of Hubble constant is the same of that of τ. Now the error is $> 50\%$.

References

[1] Gil'fanov, M. R., Syunyaev, R. A. and Churazov, E. M., 1987, Sov. Astron. Lett., 13, 3.

[2] Okumura, Y., Tsunemi, H., Yamashita, K., Matsuoka, M., Koyama, K., Hayakawa, S., Masai, K. and Hughes, J. P., 1988, ASJ, 40, 639.

[3] Molendi, S., Matt, G., Antonelli, L. A., Fiore, F., Fusco-Femiano, R., Kaastra, J., Maccarone, C. and Perola, C., Astrophys. J. 499, 608, 1998.

[4] Buote, D. A., Canizares, C. R. and Fabian, A. C., 1999, Mon. Not. R. Astron. Soc., 310, 483.

[5] Dotani, T, Yamashita, A., Ezuka, H., Takahashi, K, Crew, G., Mukai, K. and the SIS team, 1997, *ASCA* News Letter No.5.

[6] Gendreau, K. and Yaqoob, T., 1997, *ASCA* News Letter No.5.

[7] Dupke, R. A. and White, Raymond E. III, 2000, Astrophys. J., 528, 139.

[8] Nomoto, K., Iwamoto, K., Nakasato, N., Thielemann, F. K., Brachwitz, F., Tsujimoto, T., Kubo, Y. and Kishimoto, N., 1997, Nuclear Physics A, vol. A621, 467.

[9] Nomoto , K., Hashimoto, M., Tsujimoto, T., Thielemann, F. K., Kishimoto, N., Kubo, Y. and Nakasato, N., 1997, Nuclear Physics A, vol. A616, 79.